JOURNAL OF CATALYSIS 135, 596–608 (1992)

A Study of the Ni–Sb Interaction in a Rare-Earth Y-Zeolite

M. R. GOLDWASSER, D. ROJAS, AND J. GOLDWASSER[1]

Escuela de Química, Facultad de Ciencias, Universidad Central de Venezuela, Apartado 47102, Los Chaguaramos, Caracas 1050, Venezuela

Received August 19, 1991; revised December 17, 1991

Two series of catalysts were prepared by impregnating nickel and nickel–antimony over a rare-earth-exchanged Y-zeolite. The nickel loadings for the monometallic catalysts were within 0.00–1.00% in weight; for the bimetallic systems the Ni loadings were in the 0.10–0.99% range while the Sb loadings were within 0.042–0.84% in weight. The effect of Sb addition on the structure and chemisorptive properties of Ni was examined using reduction studies, CO and H_2 chemisorption, IR spectroscopy, and cracking of isooctane. Complete reduction to metallic nickel and metallic antimony was found for Ni- and Sb-rich catalysts. The addition of Sb dramatically decreased the chemisorption of H_2 and CO. Infrared results suggest the formation of a single species, probably a $Ni(CO)_x$ species, for high-loading (>0.3%) nickel catalysts (even after desorption of the gaseous CO at room temperature). For the Ni–Sb catalysts the bands were much weaker (in the presence of gaseous CO) and practically disappeared after the evacuation procedure. The cracking of isooctane showed a considerable increase in the formation of coke and hydrogen with increasing Ni loadings. The presence of antimony restored the amounts of coke and hydrogen to the original values present in the unsupported zeolite. Site blockage of Ni by Sb and weakening of the Ni–C bond by the addition of Sb are suggested to explain the results.

INTRODUCTION

As a result of increasing demand for gasoline there is a growing interest in processing heavier fractions of crude oil (*1, 2*). This can be achieved through the fluidized catalytic cracking process (FCC). Most FCC catalysts contain 15 to 25% of zeolite in a matrix of silica, alumina and/or aluminosilicates, and synthetic or natural clays. A common problem found in the FCC units is the gradual loss of catalytic performance due to the deposition of metal contaminants contained in the hydrocarbon feedstocks, e.g., Ni, V, and Fe (*3, 4*). These metals promote undesirable side reactions producing large amounts of coke and hydrogen. A possible way to overcome this difficulty involves the use of passivating agents, particularly organoantimony compounds (*1, 5, 6*). This has been shown to strongly reduce the effect of poisoning by nickel (*1*).

The interaction of Sb with Ni has been the subject of detailed studies. Dreiling and Schaffer (*6*) examined catalysts having nickel loadings in the range of 1.9–4.4% in weight and Sb : Ni ratios varying from 0.00 to 0.41. From X-ray diffraction results the authors suggested the formation of Ni–Sb solid solutions with a high level of Sb present on the nickel surface. Geometric and electronic effects were invoked to explain the results.

Parks *et al.* (*7*), working with different types of Ni and Ni–Sb catalysts, suggested the formation of an antimony-rich alloy. Hydrogen chemisorption was effectively poisoned by the presence of antimony. XPS showed that both antimony and nickel were present on surface sites with different degrees of reducibility. In view of their findings, the authors proposed (a) geometric blocking of nickel sites by the antimony present in the catalyst, (b) alteration of the electronic properties of Ni surface atoms by the presence of Sb in such a way that their catalytic activity was significantly reduced, and (c) that the amount of antimony avail-

[1] To whom correspondence should be addressed.

0021-9517/92 $5.00

able to passivate the nickel is determined by the equilibrium between Sb interacting with the support and with nickel.

The purpose of the present work is to clarify the role of Ni and Ni–Sb deposited over one of the components of a commercial FCC catalyst, a rare-earth-exchanged Y-zeolite. The results obtained in this study will be correlated, in a future work, with data obtained on real FCC catalysts.

The following techniques were used in this study. H_2 and CO chemisorption were performed to measure metal exposure. CO adsorption followed by IR spectroscopy was carried out to ascertain possible electronic and geometric effects. X-ray photoelectron spectroscopy was used as a complementary technique for the characterization of the metal phase(s) of the catalyst. The cracking of isooctane was used as a test reaction, and the influence of the nickel loading as well as the passivating effect of Sb on the conversion and selectivity patterns were studied.

EXPERIMENTAL

Catalysts

A commercial REY-zeolite (Union Carbide 720 m^2/g; SiO_2, 60.4%; Al_2O_3, 19.1%; La_2O_3, 15.8%; Na_2O, 3.9%) was heated in air at 590°C for 14 h. Various amounts of nickel (nickel naphtenate, ICN Pharmaceuticals, in toluene) were added using the standard incipient wetness technique for the impregnation procedure. The loading was varied from 0.1 to 1.0 wt% nickel.

The bimetallic catalysts were prepared in a similar fashion by coimpregnation with different amounts of antimony (di-*n*-propylthiophosphate, ICN pharmaceuticals) and nickel (0.10–0.99% Ni, 0.042–0.84% Sb) using toluene as solvent.

The catalysts were dried for 1 h at 100°C and calcined for 14 h at 590°C. The chemical analysis was performed using atomic absorption spectroscopy. The catalyst nomenclature and the analytical data are summarized in Table 1.

Procedures

H_2 and CO chemisorption experiments were performed in a conventional BET system similar to that used in Refs. (*8, 9*). Catalyst samples of approximately 0.4 g were placed in a glass microreactor and reduced *in situ* with pure hydrogen (60 cm^3(STP)/min) for 16 h at 550°C. After evacuating the catalysts at the same temperature for 1 h the H_2 adsorption isotherms were obtained at room temperature. The H_2 uptake was obtained by extrapolation of the isotherm to zero pressure (*10, 11*). The technique of Yates and Sinfelt (*12*) was used to measure CO chemisorption. In short, this method involves two CO isotherms; the irreversibly held CO is calculated from the difference of both isotherms at a pressure of 100 Torr.

The percentage reduction to the metal phase was determined from the oxygen uptake at 530°C (*13*). This temperature was sufficient to quantitatively reoxidize nickel to Ni(II) and antimony to Sb(V).

Infrared spectra were recorded at room temperature on a Perkin–Elmer 1760X Fourier transform spectrometer with a resolution of 2 cm^{-1}. The IR cell described previously (*14*) had a built-in furnace which was used to pretreat samples *in situ* at high temperatures. Samples were mounted in the cell as wafers having a thickness of approximately 20 mg/cm^2.

After the reduction procedure described previously, the CO chemisorption studies were carried out as follows: 10–40 Torr of pure CO was admitted into the cell at room temperature and the spectrum was recorded after 3 min and after 8 h. The sample was then evacuated for 30 min and the spectrum was recorded again. Integrated intensities (absorbances) were normalized to unit wafer thickness (mg/cm^2) and corrected for differences in loading (mg_{Ni}/mg of catalyst).

The procedure used for the ESCA (XPS) experiments is identical to that described in Ref. (*14*). A sealable probe allowed the transfer of the reduced catalyst from the vacuum system to the spectrometer. The ESCA spectra were generated using an AEI

TABLE 1

Chemical Composition and Chemisorption Results

Catalyst	Ni (%)	Sb (%)	Percentage[a] reduction	Chemisorption (μmol/g_{cat})		Chemisorption Adsorbate/(Ni_r)[b]	
				H_2	CO	H/Ni_r	CO/Ni_r
CT_1	0.10	—	57	0.34	0.91	0.070	0.08
CT_2	0.30	—	75	4.99	17.4	0.26	0.40
CT_3	0.50	—	100	16.6	60.5	0.39	0.71
CT_4	1.00	—	100	32.4	119	0.38	0.70
CT_5	0.10	0.042	—	—	—	—	—
CT_6	0.29	0.28	—	—	—	—	—
CT_7	0.49	0.31	100	1.25	3.34	0.030	0.041
CT_8	0.99	0.84	100	3.37	6.74	0.040	0.040

[a] Percentage reduction calculated by reoxidation assuming Ni(II) and Sb(V) as final oxidation states. For details see text.

[b] Based on amount of reducible nickel (Ni_r). For the bimetallic catalysts the chemisorption per reduced nickel atom is given.

ES200A spectrometer described previously (*14*). The Si 2*p* line (103.2 eV) of the zeolite was used as an internal standard for determination of binding energies (*7*).

Catalytic studies were carried out in a conventional continuous flow system (*15*). Isooctane was placed in a saturator, the temperature of which was set by means of a thermostated bath. A flow of nitrogen transported the isooctane to the catalyst bed maintained at constant temperature (±0.2°C). The isooctane pressure was 771.4 Torr. The reactor was 18 cm long, 2 cm i.d., and made of stainless steel. The reaction products were analyzed by on-line gas chromatography, using a Perkin–Elmer Sigma 3B chromatograph with a flame ionization detector, and separated onto a 20% Squalane/Firebrick column (4 m, 2 mm i.d.) at 90°C.

CH_4 and H_2 were analyzed with a thermal conductivity cell Varian 3700 chromatograph, using silica gel (3 m) and molecular sieve 5A (2 m) columns at room temperature. The coke produced during the reaction was followed gravimetrically.

The catalytic results are reported in terms of the total conversion (fraction of isooctane reacted per mole fed) and the percentage product formation (mole percentage of a particular product or group of products, e.g., C_1, C_3, etc).

Reactants

Hydrogen was purified by being passed through a molecular sieve and commercial Deoxo traps to remove water and oxygen traces (*8*). CO and O_2 were purified according to Ref. (*14*). Isooctane was BDH reagent grade, and gas chromatography showed no impurities.

RESULTS

Chemisorption and Reduction Studies

Table 1 gives the results for the chemical composition, percentage reduction, and chemisorptive properties of the catalysts studied. The CO admission to the reactor was performed in a very slow fashion since it has been shown earlier (*16*) that high uptake values can be obtained otherwise. A very small decline in pressure was observed during the adsorption of CO (in particular for catalysts CT_3 and CT_4) after equilibration for 30 min. This could be due to the reported formation of subcarbonyl species (*17*).

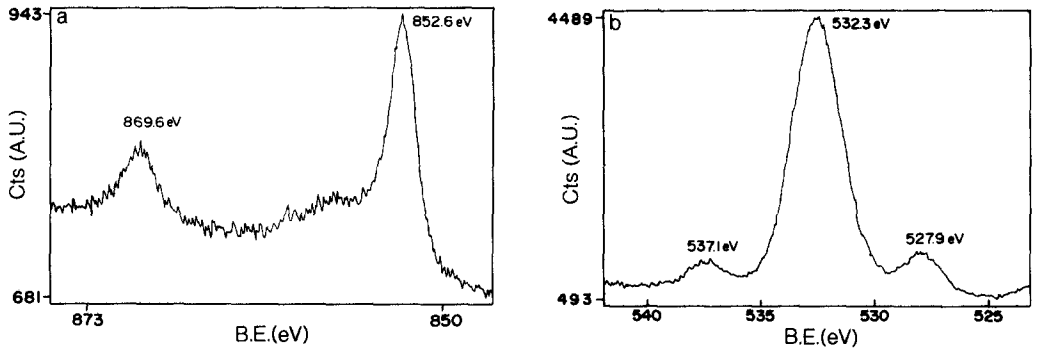

FIG. 1. ESCA spectra for the CT_8 catalyst. (a) Nickel $2p$ spectrum, (b) antimony $3d$ spectrum.

For the monometallic catalysts, Table 1 shows an increase in the H_2 and CO chemisorption with increasing Ni loading up to 1%. A dramatic decrease in CO and H_2 uptakes is observed when Sb is added to the catalysts. The calculated extent of reduction shows a complete reduction for CT_3, CT_4, CT_7, and CT_8 catalysts, whereas the low-loading Ni catalysts CT_1 (0.10%) and CT_2 (0.30%) underwent 57 and 75% reductions, respectively.

ESCA Studies

ESCA experiments were conducted in order to ascertain the possible oxidation states of the metallic components following the reduction treatment. Figure 1 shows the ESCA results for catalyst CT_8. The peaks at 852.6 and 869.6 eV (Fig. 1a) correspond to the characteristic doublet $2p_{3/2}$ and $2p_{1/2}$ for metallic nickel (*18*). The doublet located at 527.9 and 537.1 eV (Fig. 1b) can be assigned to the $3d_{5/2}$ and $3d_{3/2}$ transitions for metallic Sb (*18*). The results obtained, in the nickel region, for the CT_8 sample were very similar to those obtained for the CT_4 catalyst. The signal observed at 532.3 eV corresponds to the oxygen $1s$ peak.

Infrared Results

Infrared experiments using CO as the probe molecule were carried out at room temperature according to the protocol described in the Experimental section. Figures 2 and 3 show the results obtained for the CT_1 and CT_3 samples. Prior to the adsorption of CO (Figs. 2a and 3a) the catalysts showed two bands at ca. 1610 and 1840 cm^{-1}. After addition of CO five prominent peaks, designated *A*, *B*, *C*, *D*, and *E* (Table 2), were observed in the CO region of the IR spectra.

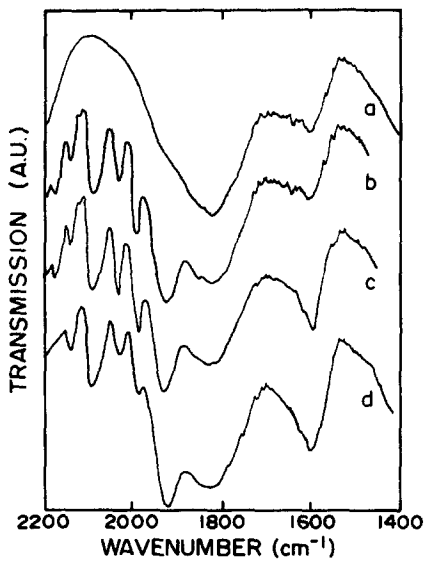

FIG. 2. Infrared spectra of carbon monoxide adsorbed on the CT_1 catalyst (a) before adsorption of CO, (b) after adsorption of CO for 3 min, (c) after adsorption of CO for 8 h, (d) after evacuation at room temperature for 30 min following procedure c.

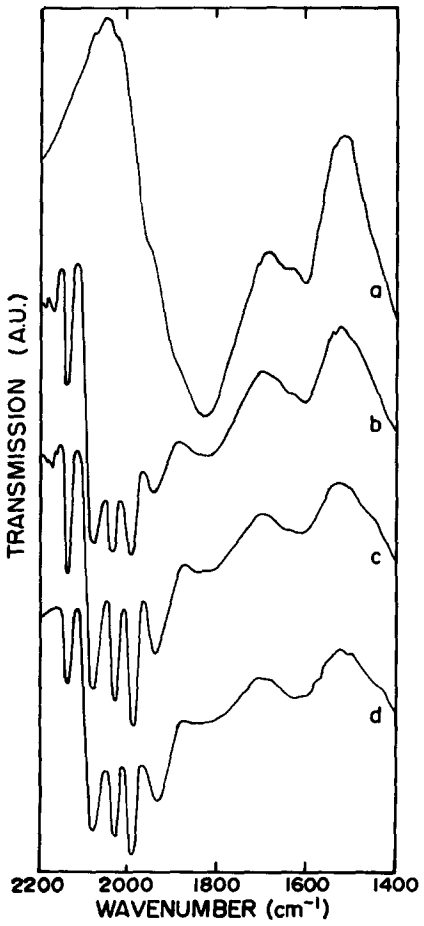

FIG. 3. Infrared spectra of carbon monoxide adsorbed on the CT_3 catalyst (a) before adsorption of CO, (b) after adsorption of CO for 3 min, (c) after adsorption of CO for 8 h, (d) after evacuation at room temperature for 30 min following procedure c.

TABLE 2

Frequency assignments of IR Bands Obtained by Adsorbing CO on Nickel and Nickel–Antimony Catalysts

Catalyst	Wavenumber/cm^{-1}					
	A	*B*	*C*	*D*	*E*	Other bands
(I) CT_1[a]	1930	1993	2031	2089	2141	2172, 2185
(II) CT_1[b]	1933	1992	2031	2086	2141	2172, 2186
(III) CT_1[c]	1927	1990	2031	2090	2141	— —
(I) CT_2	1931	1993	2031	2088	2141	2188
(II) CT_2	1937	1994	2031	2079	2138	2188
(III) CT_2	1935	1994	2031	2083	2140	—
(I) CT_3	1941	1994	2031	2078	2135	2180, 2190
(II) CT_3	1943	1994	2031	2076	2134	2180, 2190
(III) CT_3	1940	1994	2031	2079	2137	— —
(I) CT_4	1948	1993	2032	2078	2132	2175
(II) CT_4	1948	1991	2032	2079	2132	2175
(III) CT_4	1944	1992	2032	2079	2132	—
(I) CT_7	1935	1983	2033	2079	2140	2163, 2186
(II) CT_7	1940	1993	2031	2071	2139	2173, 2187
(III) CT_7	—	—	—	—	—	2061
(I) CT_8	1945	1988	2030	2079	—	2168, 2186
(II) CT_8	1941	1991	2030	2077	2135	2057
(III) CT_8	—	—	—	—	—	2062

[a] After adsorption of CO for 3 min.

[b] After adsorption of CO for 8 h.

[c] After evacuation for 30 min following adsorption of CO for 8 h (footnote *b*). The same procedure was followed for all the catalysts studied.

The *A* band shows the largest shift in frequency when the nickel loading is increased (1927 cm^{-1} for the CT_1 catalyst and 1944 cm^{-1} for the CT_4 sample). *B* and *C* bands remain constant while *D* and *E* bands show a moderate decrease in frequency when the nickel loading is increased from 0.1 and 0.3%, respectively. In addition to the abovementioned five bands other minor peaks in the high-frequency range from 2170 to 2190 cm^{-1} were observed. These bands disappeared upon evacuation at room temperature.

Table 3 shows the integrated intensities for various bands. For CT_1 catalyst, *A* is the most intense band, particularly after evacuation of the catalyst at room temperature. For catalysts CT_2, CT_3, and CT_4 the integrated intensities per gram of total nickel for *B*, *C*, *D*, and *E* bands show an increase in intensity with increasing nickel loading. This increase is considerably more moderate for the *A* band. For CT_2–CT_4 catalysts *B*, *C*, and *D* bands have similar intensities (after adsorption of CO for 8 h and desorption at room temperature) whereas the *A* band is the weakest.

Figure 4 and Table 2 show the IR results for the CT_8 bimetallic catalyst. In this case very weak bands appear after adsorption of CO for 3 min (Fig. 4b). After 8 h of adsorption (Fig. 4c) the bands become more intense; their frequencies are very similar to

TABLE 3

Integrated Intensities[a] of IR Bands Obtained by Adsorbing CO on Nickel and Antimony Catalysts

Catalyst	*A*	*B*	*C*	*D*	*E*	
(I) CT_1[b]	702	510	395	555	160	
(II) CT_1[c]	816	580	430	600	180	
(III) CT_1[d]	580	150	100	350	120	
(I) CT_2	545	510	492	621	96	
(II) CT_2	889	1371	1304	1304	300	
(III) CT_2	666	990	967	999	200	
(I) CT_3	823	1851	1880	1780	286	
(II) CT_3	1004	2610	2430	2350	602	
(III) CT_3	723	1948	1827	1736	481	
(I) CT_4	861	1804	1810	1790	290	
(II) CT_4	1100	2410	2360	2280	800	
(III) CT_4	830	1850	1720	1640	551	
(I) CT_7	—	—	—	—	—	
(II) CT_7	194	131	164	266	41	
(III) CT_7	—	—	—	—	—	
(I) CT_8	—	—	—	—	—	127[e]
(II) CT_8	70	172	162	172	36	
(III) CT_8	—	—	—	—	—	122[f]

[a] Integrated intensities normalized to unit wafer thickness (mg/cm^2) and given in arbitrary units per gram of total nickel.

[b,c, and d] Same as footnotes [a], [b], and [c] of Table 2, respectively.

[e] Integrated intensity for the 2061 cm^{-1} band.

[f] Integrated intensity for the 2062 cm^{-1} band.

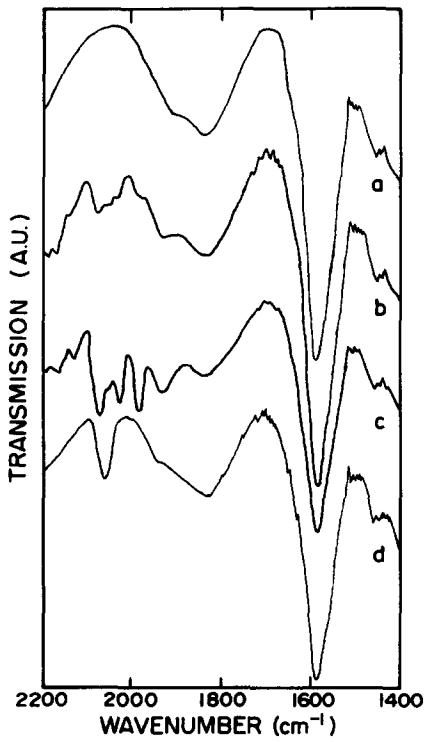

FIG. 4. Infrared spectra of CO adsorbed on the CT_8 catalyst (a) before adsorption of CO, (b) after adsorption of CO for 3 min, (c) after adsorption of CO for 8 h, (d) after evacuation at room temperature for 30 min following procedure c.

those found in the monometallic systems. After evacuating the cell for 30 min at room temperature the reported bands disappear and a weak band at 2062 cm^{-1} emerges. The results for the integrated intensities are summarized in Table 3. The changes brought about by the addition of antimony are evident.

Catalytic Studies

Preliminary experiments were performed to determine the reaction conditions for maximum steady-state catalytic activity for the cracking of isooctane. The influence of parameters such as reaction temperature and space time was studied. Thereafter, the effect of Ni loading was determined under the previously selected experimental conditions followed by the study of the effect of Sb addition in these catalysts. The reaction products obtained were methane, propane, propene, isobutane, isobutene, *cis*- and *trans*-2-butene, and H_2.

The influence of the reaction temperature over the activity of the REY-zeolite was determined between 350 and 550°C. As can be seen in Fig. 5 a significant increase in the yield of isobutane and isobutene was observed at 450°C. A similar behavior was obtained for the Ni and Ni–Sb impregnated catalysts. With respect to the effect of the space time (W/F), the yield of isobutane increases to 3.9 mg. min. ml^{-1} (Fig. 6). At higher space times a significant deactivation of the catalyst is observed concomitant with a higher coke formation.

The effect of Ni and Ni–Sb loadings over

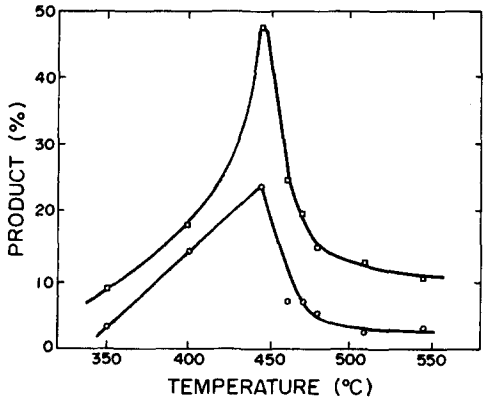

FIG. 5. Product vs reaction temperature plot for the cracking of isooctane over the REY-zeolite. (□), Isobutane, (○), isobutene.

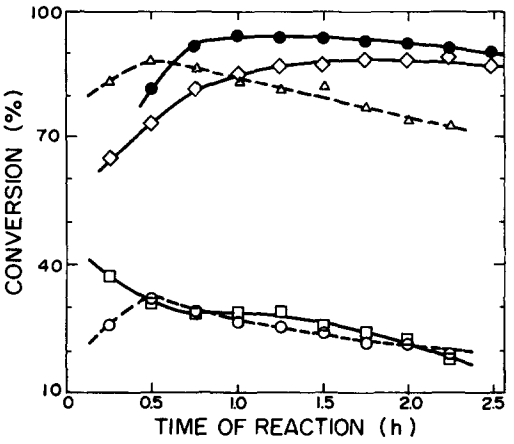

FIG. 7. Conversion vs time of reaction plot for the (◇) REY-zeolite, (□) the CT_2 catalyst, (○) the CT_3 catalyst, (△) the CT_5 catalyst, and (●) the CT_6 catalyst.

the activity–selectivity pattern of the REY-zeolite is shown in Fig. 7 and Table 4. Typically, the catalysts showed an initial increase in activity with on-stream time up to 60 min. This behavior, exhibited by most of the catalysts studied, is consistent with earlier reports (*19*).

The following changes (with respect to the unpromoted zeolite) were observed when the nickel loading was increased: (a) a strong decrease in the percentage conversion (Fig. 7), (b) a decrease in the isobutane/isobutene ratio (Table 4), (c) a decrease in the percentage of C_4 hydrocarbons (Table 4), (d) an increase in the yield of hydrogen (Table 4), and (e) an increase in the amount of coke produced (Table 4). The addition of antimony restores the conversion (Fig. 7) and the production of hydrogen and coke (Table 4) originally obtained with the unpromoted zeolite.

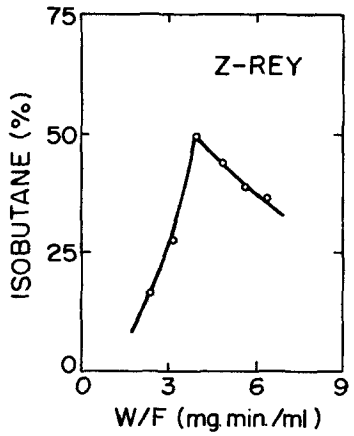

FIG. 6. Isobutane vs space time plot for the cracking of isooctane over the REY-zeolite.

DISCUSSION

The chemisorption, spectroscopic, and catalytic results shown in this work indicate that drastic changes do occur when antimony is added to the catalyst. To better understand this phenomenon, it is necessary to examine the changes that occur when nickel is impregnated on the REY-zeolite.

Previous studies have shown that the extent of reduction of nickel in alumina-supported catalysts increases with increasing nickel loading (*17*) and increasing reduction temperature (*13*). Bartholomew and Pannell (*17*) reported 29% reduction for a 0.5% Ni/Al_2O_3 catalyst and 75% reduction for a 9% Ni/Al_2O_3 catalyst reduced at 450°C. For $Ni–SiO_2$ catalysts the extent of reduction is usually higher than that for alumina-supported systems (*16, 17, 20*), due to a lower interaction with the support.

TABLE 4

Product Distribution Obtained from the Cracking of Isooctane over REY-Zeolite, Ni-REY-Zeolite, and Ni-Sb-REY-Zeolite Catalysts

Catalyst	C_1[a]	C_3[a]	C_4[a]	H_2[b]	Coke[c]	Isobutane/Isobutene
REY-Z	0.33	2.14	76.4	3.05	2.78	2.22
Ni-REY						
CT_1	1.54	4.25	57.4	4.23	3.81	1.90
CT_2	0.49	3.37	20.2	6.20	5.10	0.90
CT_3	0.36	4.24	23.2	7.31	6.20	0.71
CT_4	1.11	5.59	21.2	8.96	7.15	—
Sb-REY						
CT_5	1.24	3.96	74.3	4.45	3.51	2.27
CT_6	2.82	5.91	73.5	4.03	3.20	2.43
CT_7	2.61	6.05	63.3	3.02	2.51	2.63
CT_8	1.23	3.93	46.5	3.02	2.10	2.70

[a] Values expressed in molar percentages of C_1, C_3, and C_4 hydrocarbons.
[b] H_2 molar percentage.
[c] Coke formation was determined gravimetrically; results are given in weight percentage of coke produced.

Several studies (*21–28*) indicate that for nickel-zeolites, prepared by ion exchange, the reduction process is sensitive to temperature, H_2 pressure, treatment time, pretreatment conditions, Si/Al ratio, the presence of electron acceptor centers, and concentration of protons in the zeolite. Ni crystallites located in the supercages are assumed to interact strongly with the support. Those formed outside the framework interact in a much weaker fashion with the zeolite.

Our high-loading nickel catalysts were completely reduced (Table 1) under our experimental conditions. This result is not surprising since our catalysts were prepared using the standard incipient wetness technique for the impregnation procedure. In this case, a large fraction of nickel remains outside the zeolite framework (*22*), therefore, facilitating the reduction to metallic nickel. The low-loading catalysts CT_1 and CT_2 did not undergo total reduction, probably due to the interaction with electron acceptor sites of the zeolite (*21, 22*).

The main reason for preparing the catalysts by the standard impregnation method was to resemble, as closely as possible, the deposition of metal contaminants (contained in the hydrocarbon feedstocks) over the REY-zeolite (*29*).

Recently, Cadet *et al.* (*30, 31*) studied the reduction of nickel supported over a LaHY-zeolite (0.44% Ni) and other catalytic materials. The TPR profiles for the LaHY-catalyst showed two peaks, a small one located at 430°C and a large peak at 730°C. According to the authors, the low-temperature peak was originated by the reduction of nickel oxide-like particles while the high-temperature signal was assigned to the reduction of a nickel aluminate-like phase. The differences observed in our study, in which complete reduction for a 0.5% Ni catalyst was observed at 550°C, with the work of Cadet *et al.* (*30*) can be explained in terms of (a) different reduction conditions (5% of H_2 in argon was used in their work, and (b) different heating pretreatments (in the work of Cadet *et al.* (*30*), a hydrothermal aging with 100% steam at temperatures above 750°C was used). Under these conditions, the amount of surface nonframework aluminum, which may form a difficult to reduce nickel aluminate-like phase, increases (*31, 32*).

The chemisorption results (Table 1)

showed an increase in the CO and hydrogen uptake with increasing Ni loadings up to 0.5%. The CO_{ads}/H_{ads} ratio ranged from 1.14 to 1.84. In the absence of gaseous or weakly adsorbed nickel carbonyl formation CO_{ads}/H_{ads} ratios greater than 1 indicate adsorption of more than one CO molecule per nickel surface atom (*17, 33*). Interestingly enough, the mentioned ratio was weakly dependent on the nickel loading for the CT_2–CT_4 catalysts.

Bartholomew and Pannell (*17*) studied a series of nickel/alumina and nickel/silica catalysts of various compositions. For the nickel–alumina series a decrease in the CO_{ads}/H_{ads} ratio with an increase in the metallic loading was observed, with values ranging from 28 for 0.5% Ni/Al_2O_3 to 9.9 and 0.8 for 1 and 23% Ni/Al_2O_3) respectively. For Ni/SiO_2 catalysts the mentioned ratio was basically independent of the loading. Evidently, our results (for the high-loading catalysts) follow the trend observed for the nickel–silica system, where the metal-support interaction is rather weak (*16, 17, 20*). These results are consistent with the reduction data.

Our infrared data showed very few differences in the type(s) of species responsible for the adsorption of CO (Table 2) over the nickel catalysts studied. Five bands were always present (*A, B, C, D, E;* Table 2) and minor changes in frequencies were observed.

The normalized integrated intensities (Table 3) for the *B, C, D,* and *E* bands increase in the 0.1–0.5% range of nickel. These results are consistent with the chemisorption data since they show an increase in CO chemisorption with nickel loading. Furthermore, the intensity sequence shown for the above-mentioned bands (Table 3) is basically the same irrespective of the nickel loading. The intensity for the *A* band showed a smaller dependence on the nickel loading and did not follow the sequence observed for the other bands (i.e., for the CT_1 catalyst the *A* band was the most intense band after evacuation of CO for 30 min, while for the CT_4 catalyst the *A* band dropped to the fourth place in the intensity sequence). Thus, the species responsible for this band could be different.

Adsorption of CO on nickel-supported catalysts followed by infrared spectroscopy has been the subject of a great number of investigations (*33–42*), particularly for high-loading nickel catalysts. Bands below 2000 cm^{-1} have usually been assigned to bridged CO species, and bands above 2000 cm^{-1} have usually been assigned to linear CO and subcarbonyl species.

Wendlandt *et al.* (*43*) and Hobert *et al.* (*44*) working with 5% nickel on neutral and on strongly acidic Y-zeolites reported two different modes of adsorption of CO: the α-$Ni(CO)_4$ (2060 and 2011 cm^{-1}), in which one ligand interacts with the zeolite, resulting in a C_{3V} symmetry, and β-$Ni(CO)_4$ (2135, 2074, 2031, and 1998 cm^{-1}), in which two ligands interact with the zeolite, producing a C_{2V} symmetry. The proportion of the α-form was reported to increase with increasing zeolite acidity. The bands (in particular those at 2031 and 1998 cm^{-1}) were drastically diminished by evacuation at room temperature and no bands in the 1900–1950 cm^{-1} region were observed.

The present study shows bands similar in frequency (*B, C, D,* and *E* bands) to those of Wendlandt *et al.* (*43*) (β-$Ni(CO)_4$). Our results, however, indicate a small decrease in intensity (Table 3) for all the bands after the catalyst was evacuated for 30 min at room temperature (in particular, catalysts CT_2, CT_3, and CT_4). This result suggests the formation of a strongly held form of nickel carbonyl (or subcarbonyl) on the zeolite. This assumption is consistent with the following observations:

1. The *B, C, D,* and *E* bands behave as a set of bands belonging to a common species. For example, the changes in one peak are always accompanied by parallel changes in the other bands; the intensity sequence observed before and after evacuation at room temperature is basically the same. This is usually not observed when CO is adsorbed

as independent species with different heats of adsorption (*34*).

2. The *B* band (~1994 cm^{-1}) is very seldom present when CO is adsorbed as independent species (linear, multicenter, etc.) (*34*).

3. The addition of antimony has a similar effect on each one of the above-mentioned bands.

4. The CO_{ads}/H_{ads} ratio, which ranged from 1.54 to 1.84 (CT_2–CT_4 catalysts), is indicative of more than one CO molecule adsorbed per surface nickel (*16, 17*).

The *A* band behaved in a different way. Based on the observed frequency value, this peak could be assigned to a multicentered or bridged species (*34, 40*). This correlation is, however, doubtful since the addition of antimony (catalysts CT_7 and CT_8) does not selectively reduce the *A* band, as shown in the literature for bridge bound species (*45*). The problem remains open and deserves a more detailed study.

Ni–Sb Catalysts

Table 1 shows a dramatic decrease for the adsorption of hydrogen and CO when antimony is added to the nickel catalysts. These results agree with early literature (*7*) and can be explained in terms of a Ni–Sb alloy formation with surface enrichment in Sb (*46, 47*).

Our infrared results for the bimetallic catalysts (before evacuation of the CO) show the same set of bands observed for the nickel catalysts plus a shoulder at 2057 cm^{-1}. The intensity, however, decreases considerably from the values obtained for the monometallic catalysts (Table 3). This result is consistent with the chemisorption data. Interestingly, the shoulder at 2057 cm^{-1}, which is indicative of gaseous or weakly adsorbed $Ni(CO)_4$ (*39*), appears on the bimetallic catalysts. This fact can be understood since the addition of Sb is known to decrease the crystallite size (*6, 40*). It is known (*17, 33*) that formation of $Ni(CO)_4$ as well as subcarbonyl species is favored over small nickel particles.

Drastic changes occur when CO is evacuated at room temperature. All the bands disappear and a weak band at 2062 cm^{-1} emerges. These phenomena can be explained if the irreversible adsorption of CO is dependent on the nature of the electronic interaction between Ni and Sb during the formation of the alloy. Ni–Sb alloys are known to have a large heat of formation (−7.9 kcal/mol) (*49*). Electronic effects have been proposed in the literature (*50*) to explain the strong Ni–Sb interaction present in bimetallic systems. Due to this effect the backbonding capacity of nickel may be reduced by the presence of Sb, producing a decrease in the Ni–C bond strength, thereby decreasing the amount of chemisorbed CO.

The nature of the weak band at 2062 cm^{-1} is still under study. Presumably, a very small amount of linearly adsorbed CO (*40*), produced by decarbonylation of the ill-adsorbed species during the evacuation process, might be responsible for the mentioned band. The band position (Table 2) and the ratio $CO_{ads}/H_{ads} \simeq 1$ (Table 1) are consistent with this suggestion. More work is needed to shed light on this particular subject.

Catalytic Results

Cracking of model compounds, such as isooctane (*51*), is often used as a measure for the activity of catalysts. The behavior of the REY-zeolite follows the expected pattern characteristic of hydrocracking catalysts, namely a high yield of C_4 hydrocarbon (Table 4), indicating the presence of a primary cracking process (*52, 53*). Saturation of the formed isobutene by hydrogen transfer seems to be the only important secondary reaction. The high activity of the REY-zeolite is related to its acidity and to its open pore structure which allows the accessibility of the reactant to the active cracking sites of the zeolite (*53*). The presence of nickel on the zeolite strongly modifies the selectivity of the cracking products toward a higher production of methane and hydrogen. It also favors the formation of unsaturated compounds, which may, by

condensation, increase the amount of coke (*54*). According to O'Connor and Gevers (*1*) the hydrogen/methane ratio is strongly dependent on the amount of "active" nickel present on the catalyst. The order of magnitude increase observed in the present study with increasing nickel loadings (catalysts CT_1–CT_4, Table 4) confirms this observation.

The strong decrease observed in the percentage conversion of nickel catalysts can be explained in terms of the interaction of the nickel with the active sites of the zeolite and increased coke formation which can cause pore mouth plugging. Nickel is a promoter for cracking and coking (*29, 30*). If poisoning of the active sites by coking is more pronounced than the cracking promotion, the presence of nickel will lead to a decrease in the conversion level, as was observed.

The addition of antimony restores the production of hydrogen and coke as well as the isobutane/isobutene ratio to the values originally observed with the unpromoted zeolite. Interestingly, the hydrogen/methane ratio is strongly decreased by the presence of antimony (Table 4). Evidently, the dehydrogenating capacity of nickel is seriously diminished by Sb. This effect can be understood in terms of the formation of an exothermic Ni–Sb alloy with enrichment of antimony on the surface of the Ni–Sb_x crystallites, as proposed in the literature (*6, 7, 50*).

Finally, some observations concerning the significance of this work are in order. This study was undertaken to further clarify the surface chemistry of nickel and nickel–antimony–REY-zeolite catalysts. Although progress was made toward this objective, a legitimate question arises: How do our results relate to real FCC catalysts in which the Ni–Sb interaction might be substantially altered by the matrix? Preliminary results (*48*) obtained with FCC catalysts, prepared with nickel and nickel–antimony loadings similar to those used in this work, have shown the following: (a) the activity and selectivity trends found for the cracking of isooctane were similar to those obtained in this work. The addition of Sb suppressed the formation of coke and H_2 (with respect to the nickel catalysts). (b) The temperatures needed for the reduction of the nickel catalysts were higher than those found in this work, in accordance with the literature (*30*). The high-loading catalysts, as in this work, were more easily reduced than the low-loading catalysts. More work is presently under way on the FCC catalysts.

CONCLUSIONS

Ni Catalysts

1. Nickel–REY catalysts showed total reduction to metallic nickel for loadings higher than 0.3% in weight. These results differ from those reported in the literature for nickel–alumina catalysts with similar loadings.

2. The amount of chemisorbed CO and hydrogen increased with the nickel loading. The CO_{ads}/H_{ads} ratios were larger than one (for the higher Ni loadings) and showed a very small dependence on the amount of nickel. The IR experiments suggested a single species, presumably a $Ni(CO)_x$ species, strongly adsorbed.

3. The cracking of isooctane showed an increase in the amounts of coke and hydrogen produced as the nickel loading was increased. A decrease in the total conversion and C_4 yield was also observed.

Ni–Sb Catalysts

1. Catalysts CT_7 (0.49% Ni, 0.31% Sb) and CT_8 (0.99% Ni, 0.84% Sb) showed total reduction for both metals.

2. The chemisorption of hydrogen and CO was drastically reduced compared to the Ni–REY catalysts. CO_{ads}/H_{ads} ratios were close to one. The IR experiments (in the presence of gaseous CO) showed a set of bands similar to those on the Ni–REY catalysts. Their intensities were, however, greatly reduced. Evacuation at room temperature led to the disappearance of the ob-

served bands while a very weak band at ~2062 cm^{-1} emerged.

3. The addition of antimony practically restored the values of coke and hydrogen obtained with the unpromoted zeolite. The effect on the total conversion was similar. Our results can be understood in terms of the formation of an exothermic Ni–Sb alloy with surface enrichment in antimony, as proposed in the literature (*6, 7, 50*).

ACKNOWLEDGMENTS

The authors express their gratitude to Dr. D. Hercules for allowing the use of the ESCA facilities at the University of Pittsburgh, to Dr. M. Houalla for helpful discussions, and to Consejo Nacional de Investigaciones Científicas y Tecnológicas (CONICIT) for financial support. We also express our appreciation to Jose L. Galavis for providing the chemisorption data.

REFERENCES

1. O'Connor, P., and Gevers, A. W., "Proceedings, 10th Iberoamerican Symposium in Catalysis," Vol. 2, p. 1029, Mérida, Venezuela, 1986.
2. Otterstedt, J. E., Gevert, S. B., Jaras, S. G., and Menon, P. G., *Appl. Catal.* **22,** 159 (1986).
3. Ocelli, M. L., Pisaras, D., and Suib, S. L., *J. Catal.* **96,** 363 (1985).
4. Schubert, P. F., *Prepr. Am. Chem. Soc. Div. Pet. Chem.* **32,** 673 (1987).
5. McKay, D. L., and Bertus, B. J., *Prepr. Am. Chem. Soc. Div. Pet. Chem.* **24,** 645 (1978).
6. Dreiling, M. J., and Schaffer, A. M., *J. Catal.* **56,** 130 (1979).
7. Parks, G. D., Schaffer, A. M., Dreiling, M. J., and Shiblom, C. M., *Prepr. Am. Chem. Soc. Div. Pet. Chem.* **25**(2), 334 (1980).
8. Goldwasser, J., Arenas, B., Bolívar, C., Castro, G., Rodriguez, A., Fleitas, A., and Girón, J., *J. Catal.* **100,** 75 (1986).
9. Romero, T., Arenas, B., Perozo, E., Bolívar, C., Bravo, G., Marcano, P., Scott, C., Perez Zurita, M. J., and Goldwasser, J., *J. Catal.* **24,** 281 (1990).
10. Benson, J. E., and Boudart, M., *J. Catal.* **4,** 704 (1965).
11. Wilson, G. R., and Hall, W. K., *J. Catal.* **17,** 190 (1970).
12. Yates, D. J. C., and Sinfelt, J. H., *J. Catal.* **8,** 348 (1967).
13. Bartholomew, C. H., and Farrauto, R. J., *J. Catal.* **45,** 41 (1976).
14. Goldwasser, J., Houalla, M., Fang, S. M., and Hall, W. K., *J. Catal.* **115,** 34 (1989).
15. Goldwasser, M. R., Rojas, D., Franco Parra, C., Machado, F., Goldwasser, J., and Martinez, N. P., "Proceedings, 11th Iberoamerican Symposium in Catalysis," Vol. 1, p. 17, Guanajuato, Mexico, 1988.
16. Smith, J. S., Thrower, P. A., and Vannice, M. A., *J. Catal.* **68,** 270 (1981).
17. Bartholomew, C. H., and Pannell, R. B., *J. Catal.* **65,** 390 (1980).
18. Wagner, C. D., Riggs, W. H., Davis, L. E., Moulder, J. F., and Muilenberg, G. E., "Handbook of X-ray Photoelectron spectroscopy," Perkin–Elmer, MN.
19. Lagner, B. E., and Meyer, S., *in* "Catalyst Deactivation" (B. Delmon and G. F. Froment, Eds.), p. 91. Elsevier, Amsterdam/New York, 1980.
20. Tatterson, D., and Mieiville, C., *Ind. Eng. Chem. Res.* **27,** 1595 (1988).
21. Delafosse, D., *in* "Catalysis by Zeolites" (B. Imelik, C. Naccache, Y. Ben Taarit, J. C. Vedrine, G. Coudurier, and H. Praliaud, Ed.), p. 235. Elsevier, Amsterdam/New York, 1980.
22. Minachev, Kh.M., and Isakov, Ya.I., *in* "Zeolite Chemistry and Catalysis" (J. Rabo, Ed.), Monograph 171, p. 552. American Chemical Society, Washington, DC, 1976.
23. Richardson, J. T., *J. Catal.* **21,** 122 (1971).
24. Gryaznova, Z. V., Epishina, G. P., and Micheleva, I. M., *Dokl. Akad. Nawk. SSSR* **203,** 1339 (1972).
25. Jacobs, P. A., Nijs, H., Verdonck, J., Derouane, E. G., Gibson, J. P., and Simoens, A. J., *J. Chem. Soc. Faraday Trans. 1* **75,** 1196 (1979).
26. Sauvion, G. N., Djemel, S., Tempere, J. F., Guilleux, M. F., and Delafosse, D., *in* "Catalysis by Zeolites" (B. Imelik, C. Naccache, Y. Ben Taarit, J. C. Vedrine, G. Courdurier, and H. Praliaud, Eds.), p. 245. Elsevier, Amsterdam/New York, 1980.
27. Torrealba, M., Ph.D. thesis, Universidad Central de Venezuela, Caracas, Venezuela, 1991.
28. Ione, K. G., Romannikov, V. N., Davydov, A. A., and Orlova, L. B., *J. Catal.* **57,** 126 (1979).
29. Mitchell, B. R., *Ind. Eng. Chem. Prod. Res. Dev.* **19,** 209 (1980).
30. Cadet, V., Roatz, F., Lynch, J., and Marcilly, C., *Appl. Catal.* **68,** 263 (1991).
31. Cadet, V., Roatz, F., Lynch, J., and Marcilly, C., *Stud. Surf. Sci. Catal.* **49** (B), 1377 (1989); *in* "Zeolites: Facts, Figures and Future," p. 1377. Elsevier, Amsterdam/New York, 1980.
32. Dwyer, J., Fitch, F., Machado, F., Qin, G., Smyth, S., and Vickerman, J., *J. Chem. Soc. Chem. Commun.*, 422 (1985).
33. Bradshaw, A. M., and Pritchard, J., *Surf. Sci.* **17,** 372 (1969).
34. Sheppard, N., and Nguyen, T. T., *in* "Advances in Infrared and Raman Spectroscopy," (R. J. Clarke and R. E. Hester, Eds.), Vol. 4, p. 67. Wiley, New York, 1978.
35. Eischens, R. P., Pliskin, W. A., and Francis, S. A., *J. Chem. Phys.* **22,** 1786 (1954).

36. Eischens, R. P., and Pliskin, W. A., *in* "Advances in Catalysis" (D. D. Eley, W. G. Frankenburg, and V. I. Komarewsky, Eds.), Vol. 10, p. 1. Academic Press, New York, 1958.
37. Blackmond, D. G., and Ko, E. I., *Appl. Catal.* **13,** 49 (1984).
38. Yates, J. T., Jr., and Garland, C. W., *J. Phys. Chem.* **65,** 617 (1961).
39. Rochester, C. W., and Terrel, R. J., *J. Chem. Soc. Faraday. Trans. 1* **73,** 609 (1977).
40. Primet, M., Dalmon, J. A., and Martin, G. A., *J. Catal.* **46,** 25 (1977).
41. Van Hardeveld, R., and Hartog, F., "Advances in Catalysis," (D. D. Eley, H. Pines, and P. B. Weisz, Eds.), Vol. 22, p. 75. Academic Press, New York, 1972.
42. Peri, J. B., *J. Catal* **86,** 84 (1984).
43. Wendlandt, K. P., Bremer, H., Vogt, F., Reschetilowski, W. P., Morke, W., Hobert, H., Weber, M., and Becker, K., *Appl. Catal.* **31,** 65 (1987).
44. Hobert, H., Marx, R., Weber, I., Reschetilowski, W. P., and Wendlandt, K. P., *Z. Anorg. Allg. Chem.* **539,** 211 (1986).
45. Van Santen, R. A., and Sachtler, W. M. H., "Advances in Catalysis," (D. D. Eley, H. Pines, and P. B. Weisz, Eds.), Vol. 26, p. 69. Academic Press, New York, 1977.
46. Williams, F. L., and Nason, D., *Surf. Sci.* **45,** 377 (1974).
47. Wynblatt, P., and Ku, R. C., *Surf. Sci.* **65,** 511 (1977).
48. Goldwasser, M. R., Rojas, D., and Goldwasser, J., unpublished results.
49. Stein, D. F., *Annu. Rev. Mater. Sci.* **7,** 123 (1977).
50. Hudis, J., Perlman, M. L., and Watson, R. E., *Am. Inst. Phys. Conf. Proc.* **18,** 276 (1973).
51. Rojas, D., Goldwasser, M. R., Franco, C., and Martinez, N. P., *Rev. Soc. Venez. Catal.* **1,** E1 (1987).
52. Ward, J. W., *in* "Applied Industrial Catalysis" (B. E. Leach, Ed.), Vol. 3, p. 342. Academic Press, New York, 1984.
53. Arcoya, A., Gómez, P. J., Seoane, X. L., and Valenzuela, E., "Proceedings, 10th Iberoamerican Symposium in Catalysis," Vol. 2, p. 1020, Mérida, Venezuela, 1986.
54. Franco, C., Goldwasser, M. R., Fajula, F., and Figueras, F., *Appl. Catal.* **17,** 217 (1985).